1 Star formation and stellar evolution: an overview

1.1 A short history of stellar astrophysics

Since the Sun is a star it is probably correct to say that stellar astrophysics began with Newton's well-known explanation for the Keplerian laws of planetary motion. Although J. Goodricke observed the eclipsing binary variable Algol (β Persei) in 1782, it was not until 1803 that Sir William Herschel's observations of Castor proved that two stars revolve around each other owing to their mutual gravitational attraction.

The first measurements of stellar parallax were made by F. W. Bessel and F. G. W. Struve in 1838. F. Schlesinger revolutionized stellar distance determinations in 1903 when he introduced photographic parallaxes and thereby enabled astronomers to measure parallaxes to an accuracy of about 0.01 arc seconds. K. Schwarzschild initiated photographic photometry during the years 1904–8. Photoelectric photometry of stars began shortly after the photocell was invented in 1911.

J. Fraunhofer discovered Fraunhofer absorption lines in the solar spectrum in 1814 and subsequently observed similar lines in other stars. In 1860 Kirchhoff formulated the relationship between radiative absorption and emission of radiation which is known as Kirchhoff's law. The Doppler effect and Kirchhoff's law formed the conceptual basis of early studies of stellar atmospheres. The quantum theory of blackbody radiation was introduced by M. Planck in 1900. To a first approximation most stars radiate as blackbodies with superimposed absorption and emission lines. The modern theory of radiative transfer in stellar atmospheres was initiated in 1906 by K. Schwarzschild. The Henry Draper catalogue, which was published by A. Cannon and E. C. Pickering, is the best-known early catalogue of stars. It contained classifications for 225 000 stars. In 1888 H. A. Rowland used a diffraction grating to measure the solar spectrum and subsequently produced a table specifying the wavelengths of thousands of spectral lines.

E. Hertzsprung and H. N. Russell are credited with originating the well-known Hertzsprung–Russell diagram, in which absolute stellar magnitude is plotted along the vertical axis and spectral type or color temperature along the horizontal axis. The distinction between dwarf (main-sequence) stars and giants had been recognized as early as 1905 by Hertzsprung, but the importance of this distinction was not established until 1913, when Russell used improved parallax measurements to show that most observed stars in the solar neighborhood occupy a narrow strip in the H–R diagram known as the main sequence, whereas others are giants. It is now known that there are more white dwarfs in the vicinity of the solar system than giants.

In 1924 A. S. Eddington established the mass–luminosity relationship for main-sequence stars. His book *The Internal Constitution of the Stars*, which was published in 1926, was the first stellar interiors text. It contained the basic theory of stellar pulsations but did not identify the hydrogen and helium ionization zones as the driving mechanism for pulsations in Cepheids, RR Lyrae and long-period variables. Also in 1926 Fermi–Dirac statistics was formulated by E. Fermi and P. A. M. Dirac. In December of the same year R. H. Fowler used Fermi–Dirac statistics to show that electrons are degenerate in white-dwarf interiors. S. Chandrasekhar (1931a,b) introduced the relativistic, degenerate electron gas and proved that white dwarfs have a maximum mass, which is known as the Chandrasekhar mass limit. His book *Stellar Structure* (1939) discusses white dwarfs and early work on nuclear energy generation in stars. H. Bethe and C. H. Critchfield (1938) showed that the proton–proton reaction can proceed at appreciable rates in the solar interior. C. F. von Weizsäcker (1938) and H. Bethe (1939) introduced the CN cycle. The Sun's luminosity and that of other low-mass main-sequence stars is primarily caused by the proton–proton chain. The CN cycle is operative in massive main-sequence stars, giants and novae. M. Schwarzschild's influential textbook *Structure and Evolution of the Stars* (1957) contains early numerical solutions of the equations of stellar interiors including physically realistic red-giant models. Systematic discussions of nucleosynthesis were given by Burbidge, Burbidge, Fowler and Hoyle (B^2FH) (1957) and also in papers published by A. G. W. Cameron (1955, 1957). The terms s-process and r-process were introduced in the B^2FH review article. D. D. Clayton's 1968 textbook *Principles of Stellar Evolution and Nucleosynthesis* was the first stellar astrophysics textbook to include a thorough discussion of the thermonuclear reactions and nucleosynthesis. Other references can be found in Clayton's book.

The neutron is an unstable particle in free space; however, it is a stable particle in the atomic nucleus and also in neutron stars. L. D. Landau and F. Zwicky proposed the existence of neutron stars after J. Chadwick's discovery of the neutron in 1932. The first published calculation of neutron-star models using general relativity was by J. R. Oppenheimer and G. M. Volkoff (1939). Interest in neutron stars was practically dormant until after the discovery of nonsolar x-ray sources by R. Giaconni *et al.* (1962). The discovery of objects emitting periodic radio pulses by Hewish *et al.* (1968) and subsequent interpretation of these objects as rotating neutron stars with $\sim 10^{12}$ gauss magnetic fields generated a great deal of interest in neutron-star astrophysics. S. A. Colgate and R. H. White (1966) among others had predicted that neutron stars would be formed by supernova outbursts. The discoveries of the Crab and Vela pulsars in 1968 made the neutron-star interpretation of pulsars universally accepted by astronomers. In 1971 the first x-ray satellite, *UHURU*, discovered x-ray pulsars, which are neutron stars in close binary systems. This important discovery made it possible to estimate the masses of neutron stars. The discovery of the binary pulsar PSR 1913 + 16 and subsequent interpretation of its radio emission by R. A. Hulse and J. H. Taylor (1975) proved the existence of gravitational radiation.

On the basis of Newtonian gravity and the Newtonian corpuscular theory of light, Laplace (1795) argued that light could not escape from a sufficiently massive object of given radius. The concept of a black hole was therefore proposed long before Einstein's general theory of relativity appeared in 1915. Karl Schwarzschild (1916) derived his well-known general-relativistic solution for the metric outside a spherical mass almost immediately after Einstein's work was published. Oppenheimer and H. Snyder (1939) made the first general-relativistic collapse computation by calculating the collapse of a homogeneous, pressureless gas sphere. The so-called no-hair theorem states that the physical properties of a black hole can depend only on mass, angular momentum and charge. R. P. Kerr (1963) obtained a solution for rotating black holes. A major simplification of Kerr's work was made by R. H. Boyer and R. W. Linquist in 1967. The first identified stellar-mass black hole, Cygnus X-1, was among the approximately 20 x-ray sources with discovered optical companion stars known before the end of the 1960s.

Supernovae have played a unique role in the development of stellar astrophysics. Moreover, records of supernovae extend back to about 1300 BC. Tycho's supernova of 1572, which occurred at a distance of about 2500 pc, had a visual magnitude of approximately -4.0 and was therefore comparable in brightness to Venus at maximum light. Kepler's supernova of 1604 had a visual magnitude of about -3. The Crab nebula, which is M1 in the Messier catalogue of nebulae, was formed by a supernova observed by Chinese astronomers in 1054. Nearby supernova remnants associated with relatively recent prehistoric supernovae that must have been observable without a telescope are the Vela pulsar and surrounding nebula and the Cygnus Loop. The supernova whose stellar remnant is the Vela pulsar is believed to have occurred about 8000 BC, whereas the Cygnus Loop is about 15 000 years old. The supernova remnant and strong radio source Cassiopeia A, which is only about 300 years old, may not have been sighted because of extinction by dust. However, there has been speculation that it was observed by John Flamsteed in 1680. SN 1006 is another relatively young supernova remnant that is believed associated with a very bright star that flared up in the Spring of 1006. The well-known SN I and SN II classification of supernova light curves (see Chapter 11) is due to Minkowski (1941). Recent work has shown that SN I supernovae include two distinct classes, SN Ia and SN Ib. Supernova 1987A, which was the first supernova observable without a telescope since Kepler's supernova, will be discussed further in Chapter 11.

Although not observable without a telescope, SN 1885A (S. Andromeda), which occurred in M31 (Andromeda galaxy), is of special historical significance. Its visual spectrum was known to many astronomical observers, and in 1888 O. T. Sherman published the first supernova spectrum, the blue spectrum of SN 1885A, in the *Monthly Notices of the Royal Astronomical Society*.

1.2 The Hertzsprung–Russell (H–R) diagram

Because the distance to the Sun is known, the solar luminosity $L_\odot$ is determined from the measured solar flux ($\simeq 10^6\,\mathrm{erg\,cm^{-2}\,s^{-1}}$). The directions to neighboring stars change significantly as the Earth orbits about the Sun. The parallax of a star is half the angle subtended by the mean diameter of the Earth's orbit. Therefore, we have

$$\tan \alpha = \frac{1\,\mathrm{AU}}{d}, \tag{1.1}$$

with α equal to the parallax in radians, d equal to the distance and 1 AU equal to the astronomical unit (1.496×10^{13} cm), which is the average Earth–Sun distance. A parsec (pc) is defined to be the distance at which a star's parallax equals one second of arc. Since α in Equation (1.1) is small and there are 206 265 seconds of arc in one radian, the stellar distance d becomes

$$d = \left(\frac{206\,265}{p''}\right) 1\,\mathrm{AU} = \frac{1}{p''}\,\mathrm{pc}, \tag{1.2}$$

with p'' the parallax in units of seconds of arc.

The apparent-magnitude scale is defined so that the flux ratio F_1/F_2 and corresponding apparent magnitudes m_1 and m_2 are related by the equation

$$\frac{F_1}{F_2} = 10^{0.4(m_2 - m_1)}. \tag{1.3}$$

Equation (1.3) implies that a flux ratio of 10^2 corresponds to a difference of 5 magnitudes.

The absolute magnitude M is defined so that it is equal to the apparent magnitude m if the stellar distance r is equal to 10 pc. It follows that apparent and absolute magnitude are related by the equation

$$M = m + 5 - 5 \log r, \tag{1.4}$$

where r is in units of parsecs. Equation (1.4) implies that if the apparent magnitude and distance to a star are measured then the absolute magnitude is determined. Since the absolute bolometric magnitude of the Sun is 4.8, the absolute magnitude of a star of luminosity L can be expressed as

$$M - 4.8 = -2.5 \log\left(\frac{L}{L_\odot}\right), \tag{1.5}$$

with $L_\odot = 3.86 \times 10^{33}\,\mathrm{erg\,s^{-1}}$.

Magnitude scales are defined in different spectral bands. The visual apparent magnitude m_v (or V) is a measure of the flux received from a star through a standard visual filter. Blue (B) and ultraviolet (U) magnitude scales are also commonly used at optical wavelengths. Differences in magnitude as measured with visual (V), blue (B) and ultraviolet (U) filters determine the color temperature of a star. If a star has some visual magnitude and color temperature, then a bolometric correction (BC) is determined. The bolometric magnitude m_{bol} becomes

$$m_{\mathrm{bol}} = m_v + BC. \tag{1.6}$$

Interstellar dust particles scatter and absorb starlight. The amount of extinction of starlight caused by dust particles depends on a star's distance and particular location. Some stars are embedded in or behind molecular clouds, which contain large amounts of dust, and consequently extinction of optical radiation is large. In the galactic plane the average amount of extinction at visual wavelengths is $\simeq 0.5$–1 magnitude per kiloparsec. Color temperatures are not always indicative of photospheric temperatures because interstellar extinction causes reddening of starlight and also because some stars are sufficiently hot that measured color temperatures are insensitive to photospheric temperatures.

Stars are classified according to their spectral types, which in order of decreasing photospheric temperature are O, B, A, F, G, K and M. The relative strengths of various absorption lines determine the particular spectral type (or class). O stars have prominent ionized helium lines (He II). Neutral helium lines are strongest in B stars, which also have prominent hydrogen Balmer-series lines (Hα, Hβ, Hγ, . . .). Balmer-series absorption lines attain their maximum strengths in A stars. He II lines disappear in the A-star range, but the relative strengths of Ca II, Fe II and other singly ionized metal lines increase. Hydrogen lines are still quite strong in F stars. However, their strengths decrease continuously from earlier- to later-type F stars, whereas the strengths of singly ionized metal lines increase. In G stars ionized metals are dominant and hydrogen lines are much weaker than in A stars. The H and K lines of Ca II, which are the most prominent absorption lines in G stars, attain maximum strengths in K stars. Neutral metallic lines (e.g. Fe I) are appreciably stronger in K stars than in G stars. Hydrogen lines are weak in K stars and CH and CN bands are prominent. At visual wavelengths the spectra of M stars are dominated by Ti O bands.

Table 1.1 gives the response function for visual (V), blue (B) and ultraviolet (U) filters. Differences in the magnitude of a star as observed through different filters give a measure of the color temperature. Figure 1.1 shows $U - B$ plotted versus $B - V$ for main-sequence stars. Notice that this relation is not similar to that of blackbody spectra. Interstellar gas between stars and Earth produce atomic and molecular absorption lines. Diffuse lines are also observed. Interstellar atomic and molecular lines have much narrower line widths than stellar lines because interstellar gas is cold and therefore the line width of a particular transition is determined by the radiative lifetime rather than the Doppler width. Table 1.2 lists some interstellar lines. The wavelengths are given in ångströms.

Figure 1.2 shows how the strengths of various spectral lines vary with spectral type. As shown in Figure 1.3, much of the continuum opacity of the K giant Aldebaran is caused by the H^- negative ion, whereas infrared continuum absorption in the atmospheres of the much cooler M giants R. Leonis and Mira is mainly the result of water-vapor bands.

The H–R diagram is a plot of stellar luminosity (or equivalently absolute magnitude) versus photospheric temperature as determined either by spectral type or by color temperature. If the luminosities and photospheric temperatures of a sample of stars in a given volume of space are plotted in the H–R diagram, then it is found that most stars occupy a narrow region that extends from relatively low luminosity and photospheric temperature to much higher luminosity and photospheric temperature. Stars within this

Table 1.1. The response function S for the UBV system as given by Matthews and Sandage (1963).

$\lambda \times 10^{-2}$ (Å)	$S(U)$	$S(B)$	$S(V)$
30	0.025		
31	0.250		
32	0.680		
33	1.137		
34	1.650		
35	2.006	0.000	
36	2.250	0.006	
37	2.337	0.080	
38	1.925	0.337	
39	0.650	1.424	
40	0.197	2.253	
41	0.070	2.806	
42	0.000	2.950	
43		3.000	
44		2.937	
45		2.780	
46		2.520	
47		2.230	
48		1.881	0.020
49		1.550	0.175
50		1.275	0.900
51		0.975	1.880
52		0.695	2.512
53		0.430	2.850
54		0.210	2.820
55		0.055	2.625
56		0.000	2.370
57			2.050
58			1.720
59			1.413
60			1.068
61			0.795
62			0.567
63			0.387
64			0.250
65			0.160
66			0.110
67			0.081
68			0.061
69			0.045
70			0.028
71			0.017
72			0.007

Table 1.2. Interstellar lines. From Jaschek and Jaschek (1987).

Atomic lines		Molecular lines		Diffuse lines
Na I	λ3302, λ3303	CH	λ3137	λ4430*
	λ5890, λ5896		λ3143	λ5780
			λ3146	λ6284
K I	λ7665		λ3878	
	λ7699		λ3886	
			λ3890	
Ca I	λ4226		λ4300*	
Ca II	λ3933			
	λ3968	CN	λ3874	
			λ3875	
Ti II	λ3073			
	λ3229	CH	λ3745	
	λ3242		λ3957	
	λ3284		λ4232*	
Fe I	λ3720			
	λ3859			

*The most important feature.

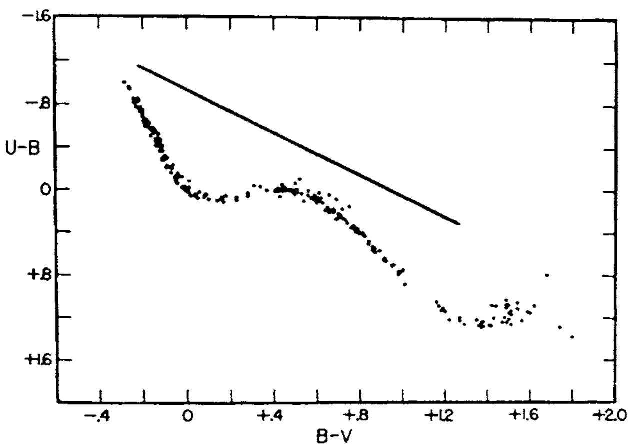

Figure 1.1. The $(U - B, B - V)$ relation for unreddened main-sequence stars. the solid line represents blackbody spectra. From Johnson and Morgan (1953).

region of the H–R diagram are known as main-sequence stars. Their luminosities are maintained by hydrogen-burning cores. Massive main-sequence stars have much higher luminosities and much shorter main-sequence lifetimes than low-mass main-sequence stars.

Figure 1.4 shows the absolute visual magnitude versus $B - V$ color temperature for nearby stars.

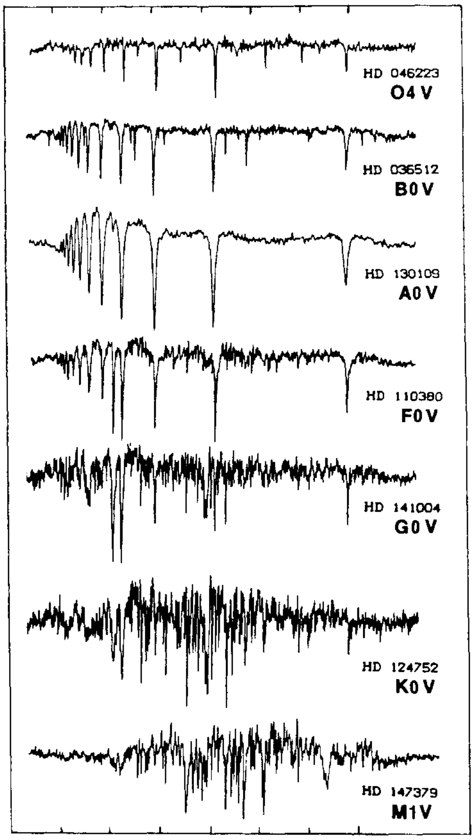

Figure 1.2. Spectra of main-sequence stars of different spectral types. From Jaschek and Jaschek (1987).

Spectral-line Doppler shifts from a binary star are shown in Figure 1.5, where it is assumed that the observer is in the plane of the orbit.

1.3 Spectroscopic binary stars

In center-of-mass coordinates the Lagrangian describing the gravitational interaction of binary stars is

$$L = \tfrac{1}{2}m(\dot{r}^2 + r^2\dot{\phi}^2) - V(r), \tag{1.7}$$

with $V(r)$ equal to the gravitational potential and $m = M_1M_2/(M_1 + M_2)$ equal to the reduced mass derived in Equation (4.5). The Lagrangian equations of motion are

$$\frac{\mathrm{d}}{\mathrm{d}t}\left(\frac{\partial L}{\partial \dot{q}_i}\right) - \frac{\partial L}{\partial q_i} = 0 \quad (i = 1, 2;\ q_1 = r, q_2 = \phi). \tag{1.8}$$

Cambridge University Press
978-0-521-58188-2 - Advanced Stellar Astrophysics
William K. Rose
Excerpt
More information

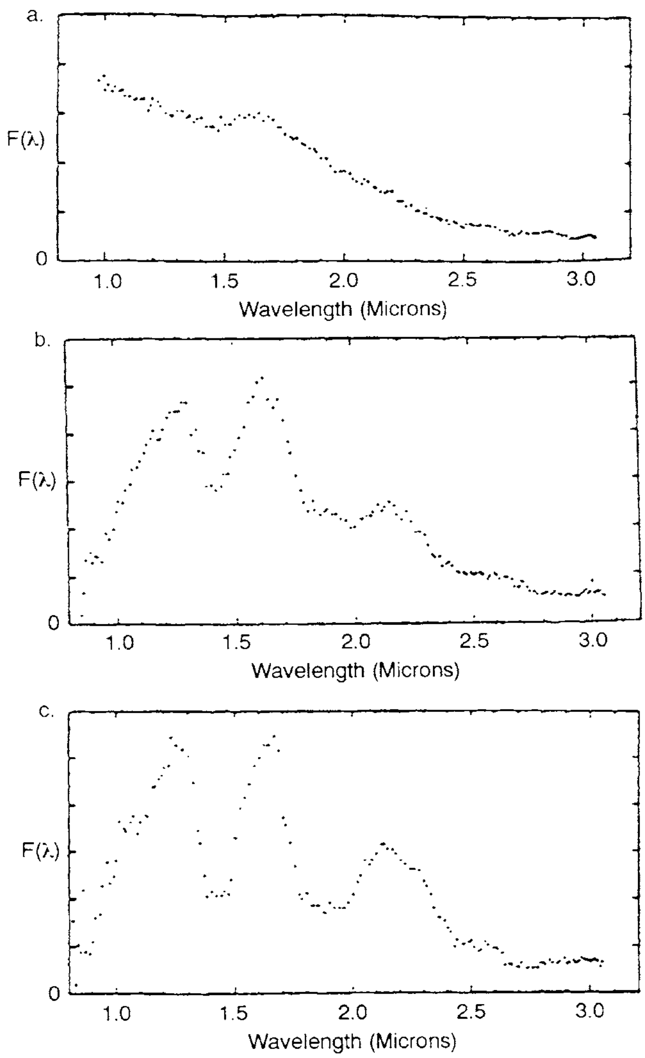

Figure 1.3. Infrared spectra of red-giant stars obtained from a balloon-borne telescope. From Woolf, Schwarzschild and Rose (1964). a. Infrared spectrum of the K5 giant α Tauri (Aldebaran). The intensity peak near 1.6 microns is where bound–free and free–free H^- absorption leaves a relatively transparent region in the continuous absorption coefficient. b. Infrared spectrum of the M8 giant R. Leonis shows evidence for water-vapor bands at 1.4, 1.9 and 2.7 microns. c. Infrared spectrum of the M9 giant σ Ceti (Mira) shows evidence for water-vapor bands at 1.4, 1.9 and 2.7 microns.

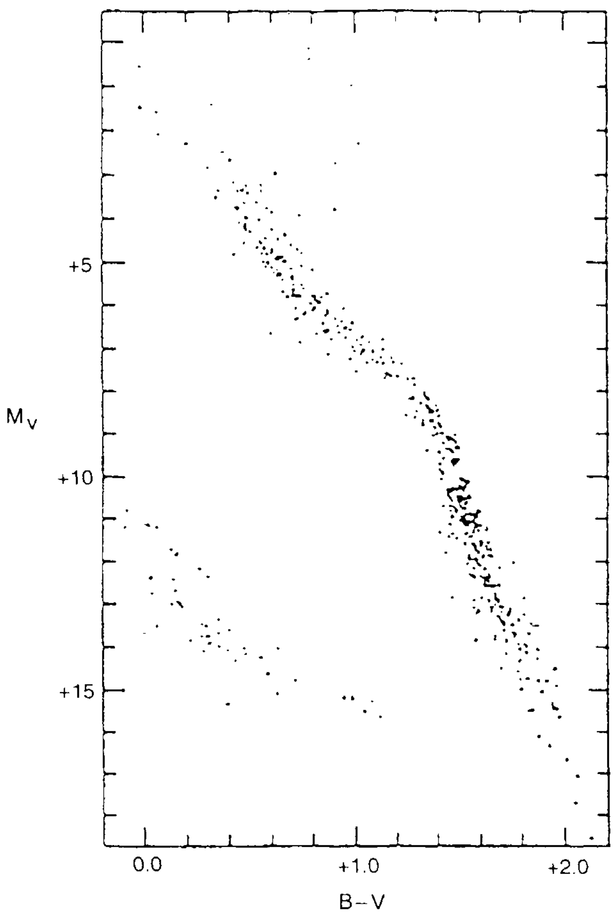

Figure 1.4. The absolute visual magnitude M_v versus $B - V$ color temperature for nearby stars (i.e. stars with trigonometric parallax ≥ 0.044 seconds of arc). White dwarfs are on the lower left and main-sequence stars above them. From Gleise (1978).

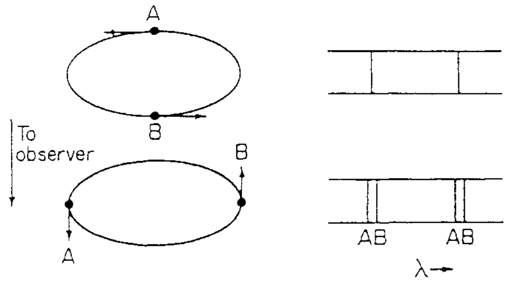

Figure 1.5. Doppler shifts of spectral lines from binary stars.